PRECISE RADIUS ESTIMATES FOR THE EXOPLANETS WASP-1b AND WASP-2b

DAVID CHARBONNEAU,[1,2] JOSHUA N. WINN,[3] MARK E. EVERETT,[4] DAVID W. LATHAM,[1] MATTHEW J. HOLMAN,[1]
GILBERT A. ESQUERDO,[1,4] AND FRANCIS T. O'DONOVAN[5]

ABSTRACT

We present precise z-band photometric time series spanning times of transit of the two exoplanets recently discovered by the SuperWASP collaboration. We find planetary radii of 1.44 ± 0.08 and 1.04 ± 0.06 R_J for WASP-1b and WASP-2b, respectively. These error estimates include both random errors in the photometry and also the uncertainty in the stellar masses. Our results are 5 times more precise than the values derived from the discovery data alone. Our measurement of the radius of WASP-2b agrees with previously published models of hot Jupiters that include both a 20 $M_\oplus$ core of solid material and the effects of stellar insolation. In contrast, we find that the models cannot account for the large size of WASP-1b, even if the planet has no core. Thus, we add WASP-1b to the growing list of hot Jupiters that are larger than expected. This suggests that "inflated" hot Jupiters are more common than previously thought and that any purported explanations involving highly unusual circumstances are disfavored.

Subject headings: planetary systems — stars: individual (WASP-1, WASP-2) — techniques: photometric

Online material: machine-readable tables

1. INTRODUCTION

The wide-field surveys for transiting exoplanets have finally begun to strike gold. For nearly 10 years, numerous groups have attempted to use small-aperture lenses to identify transits of bright stars over large patches of the sky. This turned out to be much more difficult than initially expected, and the first success was achieved only 2 years ago (Alonso et al. 2004). Since then, progress has accelerated, and in the month of 2006 September alone, three different survey teams announced the discovery of four transiting exoplanets.

The Trans-Atlantic Exoplanet Survey (TrES) reported the discovery of their second planet, TrES-2 (O'Donovan et al. 2006), the first extrasolar planet detected in the field of view of the NASA *Kepler* mission (Borucki et al. 2003) and the most massive exoplanet known to transit a nearby bright star. The HATNet project announced the discovery of HAT-P-1b (Bakos et al. 2007), a hot Jupiter orbiting one star of a visual binary, and the lowest density hot Jupiter yet detected. Most recently, the SuperWASP team announced the discovery of two planets, WASP-1b and WASP-2b (Collier Cameron et al. 2007), that are the subject of this paper. Thus, including the discovery of a planet by the XO project earlier this year (McCullough et al. 2006), four independent teams have now demonstrated the capability of identifying transiting hot Jupiters using very modest (typically 10 cm) aperture automated observatories. Several more projects also seem poised for success (for a review of current and near-future transit-search projects, see Charbonneau et al. 2007).

The reason why transiting planets are so precious, and why the exoplanet community is ebullient over the progress in finding them, is that only for transiting planets can one measure both the mass and the radius. This in turn permits one to confront observations with theoretical models of planetary structure. For the moment, this confrontation is limited to the interesting case of the hot Jupiters, for the simple reason that close-in planets are much more likely to exhibit transits.

Prior to the detection of such objects in transiting configurations, our naive expectation was that hot Jupiters would be similar to Jupiter in structure, with a modest increase in radius due to the effects of stellar insolation (e.g., Guillot et al. 1996; Lin et al. 1996). However, among the 14 cases that have since been discovered, there is a large range in measured radii. At one extreme lies HD 149026b (Sato et al. 2005; Charbonneau et al. 2006), whose small radius bespeaks a central core of solid material that composes roughly 70% of the planet by mass. At the other extreme is HD 209458b (Knutson et al. 2007), whose radius significantly exceeds the predictions of insolated structural models (see, e.g., Baraffe et al. 2003 or Bodenheimer et al. 2003, and for a contrary view, Burrows et al. 2003 or Arras & Bildsten 2006). The recently discovered planet HAT-P-1b (Bakos et al. 2007) is also larger than theoretically expected. This suggests that in those two planets, at least, there is a source of internal heat that was overlooked by theoreticians. Fortney et al. (2006) have suggested that all hot Jupiters are subject to an additional energy source, but that the effect is masked for some of these planets by a large abundance of heavy elements.

Various mechanisms for producing this heat have been explored, although certainly not exhaustively. Bodenheimer et al. (2001, 2003) proposed that there is a third body in the system that excites the eccentricity of the hot Jupiter. Ongoing tidal dissipation would then provide the requisite energy, even if the mean eccentricity were as small as a few percent. However, subsequent observations have placed an upper bound on the current eccentricity below the value required (Deming et al. 2005; Laughlin et al. 2005a; Winn et al. 2005), and they have not revealed any third body. Showman & Guillot (2002) argued instead that the heat could be provided by the conversion of several percent of the incident stellar radiation into mechanical energy that is subsequently transported deep into the planetary interior. Alternatively, Winn & Holman (2005) invoked ongoing tidal dissipation due to a nonzero planetary obliquity. Ordinarily, the obliquity would be driven

[1] Harvard-Smithsonian Center for Astrophysics, Cambridge, MA 02138; dcharbonneau@cfa.harvard.edu.
[2] Alfred P. Sloan Research Fellow.
[3] Department of Physics, and Kavli Institute for Astrophysics and Space Research, Massachusetts Institute of Technology, Cambridge, MA 02139.
[4] Planetary Science Institute, Tucson, AZ 85719.
[5] California Institute of Technology, Pasadena, CA 91107.

to very small values, but it is possible for hot Jupiters to exist in a stable Cassini state (a resonance between spin and orbital precession) with a significant obliquity.

Although measurements of either the winds or the spin states of hot Jupiters may not be forthcoming soon, a possible avenue for progress would be to examine the rate of occurrence of the anomalously large hot Jupiters relative to the hot Jupiter population as a whole (being mindful of the observational biases that favor the detection of large planets, as quantified by Gaudi 2005). In particular, the most puzzling aspect of the Showman & Guillot (2002) mechanism is why it should act on some but not all hot Jupiters. Conversely, the Cassini state described by Winn & Holman (2005) requires some fine-tuning, making it an unattractive explanation if "inflated" planets turn out to be relatively common.

Although the detection of the planets WASP-1b and WASP-2b (Collier Cameron et al. 2007) is an important opportunity to address these questions, the range of allowable planetary radii, $1.33 < R_p/R_J < 2.53$ for WASP-1b and $0.65 < R_p/R_J < 1.26$ for WASP-2b, is too broad to meaningfully constrain the models. In this paper, we present the analysis of newly acquired photometric time series that serve to reduce the uncertainties in the radii of both planets by a factor of 5. We then interpret the new radius estimates in the context of the known hot Jupiters and the published models of their physical structure. We end by noting particular opportunities for further follow-up presented by both planets.

2. OBSERVATIONS

We observed WASP-1 and WASP-2 on the nights of predicted transits, with the 1.2 m telescope of the Fred L. Whipple Observatory on Mount Hopkins, Arizona. The WASP-1 transit occurred on UT 2006 September 27, while the WASP-2 transit was on UT 2006 September 30. On each night, we used Keplercam to obtain a continuous sequence of 30 s integrations of the target and surrounding field stars. We employed the SDSS z filter, the reddest band available, to minimize the effects of differential extinction on the photometry and the effect of stellar limb darkening on the light curve. Keplercam employs a single 4096×4096 Fairchild 486 CCD; we used 2×2 binning. With a readout time of 9 s and total overhead of 12 s between exposures, the resulting cadence was 42 s. The field of view is $23' \times 23'$ with a $0.67''$ pixel^{-1} plate scale when binned. We used the offset guider to maintain the telescope pointing to within $5''$ throughout the night. On each night, we started observing well before the predicted time of ingress and ended well after egress.

For the WASP-1 event, we gathered 832 images over a time span of 9.7 hr, spanning an air mass range of $1.0-2.1$ that reached its minimum value in the middle of the observing sequence. Light clouds were present during the first hour, and conditions were photometric afterward. Since the hour in which clouds were present occurred well before ingress, we decided to exclude those data in the analysis. The full width at half-maximum (FWHM) of the stellar images was typically $1.6''$, but occasionally degraded to $4''$. For the WASP-2 event, we gathered 426 images spanning a period of 4.9 hr under clear skies and spanning an air mass that began at 1.1 and increased to 2.1 over the observing sequence. The seeing was stable, varying only modestly between $1.5''$ and $1.9''$. For calibration purposes, we obtained dome flats and twilight sky flats on both nights along with a set of bias images.

3. DATA REDUCTION

To calibrate the images, we first subtracted an amplifier-dependent overscan bias level and then joined the images from each quadrant into a single frame. We filtered the bias images from each night of deviant pixels and averaged the cleaned biases to produce an

TABLE 1
Photometry of WASP-1

HJD	Relative flux	Uncertainty
2454005.64040.....................................	1.00235	0.00204
2454005.64088.....................................	0.99903	0.00202
2454005.64138.....................................	0.99851	0.00202

Notes.—The time stamps represent the Heliocentric Julian Date at the time of midexposure. The data have been corrected for residual extinction effects, and the uncertainties have been rescaled as described in § 3. Table 1 is published in its entirety in the electronic edition of the *Astrophysical Journal*. A portion is shown here for guidance regarding its form and content. The data are also available from the authors on request.

average bias frame. We then used these average bias frames to subtract a residual spatially dependent bias pattern from the science images. We scaled our sky flat images to the same mean flux, and then averaged them (while filtering out deviant pixels) to produce nightly flat-field images, which we then used to flat-field each science image.

We performed aperture photometry using the IRAF[6] PHOT task, which yielded estimates of the instrumental magnitudes and sky magnitudes for the target and comparison stars. We estimated the sky magnitudes from the median value in an annulus centered on the star after iteratively rejecting pixel values that deviated by more than 3 standard deviations from the mean. To obtain differential photometry of the target, we selected a group of field stars that were isolated and located on a portion of the detector that was cosmetically clean. We then calculated the statistically weighted mean magnitude of the comparison stars in each frame as follows: We estimated the photometric uncertainties based on the expectations of photon noise from both the star and underlying sky, as well as detector read noise and scintillation (as formulated by Gilliland et al. 1993). We then subtracted the mean magnitude of the comparison stars from those of all stars in our list, including the target star. We eliminated from the list any comparison star found to be variable or exhibiting a systematic trend in its brightness over time. We iteratively recalculated the differential correction in this manner, eliminating suspect comparison stars until we visually confirmed in plots of the light curves that all of the comparison stars did not vary outside of the expectations of the noise sources listed above. This procedure yielded nine comparison stars for the WASP-1 data and six comparison stars for the WASP-2 data. We selected the optimal photometric aperture (which depends primarily on the typical nightly seeing) and sky annulus to be the ones that minimized the rms deviation of the out-of-transit portions of the differential light curve of the target star. We selected photometric apertures with radii of $6.4''$ and $5.4''$ for the WASP-1 and WASP-2 data, respectively. For both nights, we selected an aperture for the sky annulus that spanned $8''-21''$.

Although the relative photometry removes the first-order effects of extinction, color-dependent effects are not removed. Stars of different colors are extinguished by different amounts through a given air mass. For this reason, we applied a residual extinction correction to the data. The correction function was determined as part of the model-fitting procedure that we describe in § 4.

The final photometry is given in Tables 1 and 2, and is plotted in Figure 1. The fluxes and their uncertainties reported in the tables have already been corrected for extinction. The reported uncertainties have been further rescaled such that $\chi^2/N_{\mathrm{dof}} = 1$ for the

TABLE 2
PHOTOMETRY OF WASP-2

HJD	Relative flux	Uncertainty
2454008.60531......................................	0.99881	0.00159
2454008.60578......................................	1.00044	0.00159
2454008.60627......................................	0.99805	0.00159

NOTES.—The time stamps represent the Heliocentric Julian Date at the time of midexposure. The data have been corrected for residual extinction effects, and the uncertainties have been rescaled as described in § 3. Table 2 is published in its entirety in the electronic edition of the *Astrophysical Journal*. A portion is shown here for guidance regarding its form and content. The data are also available from the authors on request.

best-fitting model. The scaling factors were determined independently for each night, but turned out to be nearly the same: 1.28 for the WASP-1 data and 1.29 for the WASP-2 data.

4. THE MODEL

We used the same modeling techniques that have been employed previously by the Transit Light Curve (TLC) project (e.g., Holman et al. 2006; Winn et al. 2007). Our model is based on a star (with mass $M_\star$ and radius $R_\star$) and a planet (with mass M_p and radius R_p) in a circular orbit with period P and inclination i relative to the plane of the sky. We define the coordinate system such that $0° \leq i \leq 90°$. We allow each transit to have an independent value of T_c. Thus, the period P is relevant to the model only through the connection between the total mass and the orbital semimajor axis a. We fix $P = 2.51997$ days for WASP-1 and $P = 2.152226$ days for WASP-2, as determined by Collier Cameron et al. (2007). The uncertainties in P are negligible for our purposes.

The values of $R_\star$ and R_p that are inferred from the photometry are covariant with the stellar mass. For a fixed period P, the characteristics of the transit light curve depend almost exactly on the combinations $R_\star/M_\star^{1/3}$ and $R_p/M_\star^{1/3}$. Our approach was to fix $M_\star$ at the value reported by Collier Cameron et al. (2007), which they derived by comparing the spectroscopically estimated effective temperatures and surface gravities to theoretical evolutionary tracks for stars of different masses. We then used the scaling relations for the fitted radii, $R_p \propto M_\star^{1/3}$ and $R_\star \propto M_\star^{1/3}$, to estimate the systematic error due to the uncertainty in $M_\star$.

To calculate the relative flux as a function of the projected separation of the planet and the star, we assumed the limb-darkening law to be quadratic,

$$\frac{I(\mu)}{I(1)} = 1 - u_1(1 - \mu) - u_2(1 - \mu)^2, \qquad (1)$$

where I is the intensity and μ is the cosine of the angle between the line of sight and the normal to the stellar surface. We employed the analytic formulas of Mandel & Agol (2002) to compute the integral of the intensity over the unobscured portion of the stellar disk. We fixed the limb-darkening parameters u_1 and u_2 at the values calculated by Claret (2004) for a star with the spectroscopically estimated effective temperature and surface gravity. For WASP-1 these values are $u_1 = 0.1517, u_2 = 0.3530$; for WASP-2 they are $u_1 = 0.2835, u_2 = 0.2887$. We also investigated the effects of changing the limb-darkening law and allowing the limb-darkening parameters to vary in the fit (see below).

Each transit also requires two additional parameters for its description: the out-of-transit flux f_{oot} and a residual extinction coefficient k. The latter is defined such that the observed flux is
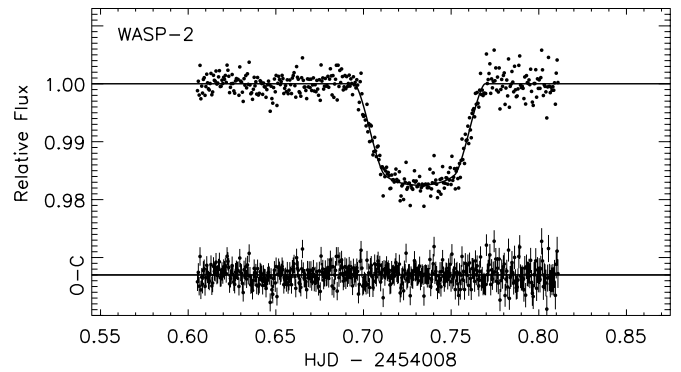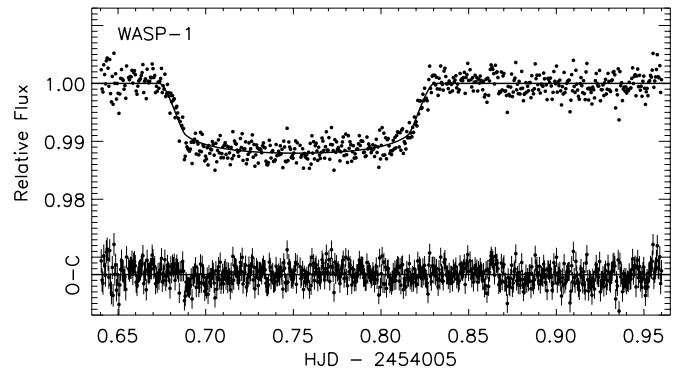

FIG. 1.—Relative z-band photometry of WASP-1 and WASP-2. The best-fitting model is shown as a solid line. The residuals (observed − calculated) and the rescaled 1 σ error bars are also shown. The residuals have zero mean but are offset for clarity by a constant flux so as to appear beneath each light curve. For both time series, the median time between exposures is 42 s, and the rms residual is 0.17%. The span of the axes is the same in both plots, permitting a visual comparison of both events. The WASP-1b transit is longer and shallower, as it corresponds to a more equatorial transit of a larger star.

proportional to $\exp(-kz)$, where z is the air mass. In total, there are six adjustable parameters for each transit: $R_\star$, R_p, i, T_c, f_{oot}, and k.

Our goodness-of-fit parameter is

$$\chi^2 = \sum_{j=1}^{N} \left[\frac{f_j(\text{obs}) - f_j(\text{calc})}{\sigma_j} \right]^2, \qquad (2)$$

where $f_j(\text{obs})$ is the flux observed at time j, σ_j is the corresponding uncertainty, and $f_j(\text{calc})$ is the predicted model value. The WASP-1 data set has $N = 657$ points (after excluding points at the beginning of the sequence, as described in § 2), and the WASP-2 data set has $N = 426$ data points. As noted in § 3, we took the uncertainties σ_j to be the calculated uncertainties after multiplication by a factor specific to each night, such that $\chi^2/N_{\text{dof}} = 1$ when each night's data were fitted independently.

We began by finding the values of the parameters that minimize χ^2, using the venerable AMOEBA algorithm (Press et al. 1992, p. 408). Then we estimated the a posteriori joint probability distribution for the parameter values using a Markov chain Monte Carlo (MCMC) technique (for a brief introduction, consult Appendix A of Tegmark et al. 2004). In this method, a chain of points in parameter space is generated from an initial point by iterating a jump function, which in our case was the addition of a Gaussian random number to each parameter value. If the new point has a lower χ^2 than the previous point, the jump is executed; if not, the jump is only executed with probability $\exp(-\Delta\chi^2/2)$. We set the typical sizes of the random perturbations such that

TABLE 3
SYSTEM PARAMETERS OF WASP-1

Parameter	Value	Uncertainty
$R_\star/R_\odot$	1.453	0.032
$R_p/R_{\rm J}$..	1.443	0.039
$R_p/R_\star$...	0.10189	0.00093
i (deg).....................................	>86.1	(95% confidence)
b..	<0.336	(95% confidence)
$t_{\rm IV} - t_{\rm I}$ (hr)	3.773	0.031
$t_{\rm II} - t_{\rm I}$ (min)	21.5	1.1
T_c (HJD)...............................	2454005.75196	0.00045

NOTES.—The parameter values in the second column are the median values of the MCMC distributions, and the uncertainties in the third column are the standard deviations. These are for a *fixed* choice of $M_\star = 1.15\ M_\odot$ and for a *fixed* choice of the limb-darkening function (see the text). The 15% uncertainty in $M_\star$ introduces an *additional* 5% uncertainty in $R_\star$ and R_p (and has no effect on the other parameters).

TABLE 4
SYSTEM PARAMETERS OF WASP-2

Parameter	Value	Uncertainty
$R_\star/R_\odot$	0.813	0.032
$R_p/R_{\rm J}$..	1.038	0.050
$R_p/R_\star$...	0.1309	0.0015
i (deg).....................................	84.74	0.39
b..	0.731	0.026
$t_{\rm IV} - t_{\rm I}$ (hr)	1.799	0.035
$t_{\rm II} - t_{\rm I}$ (min)	24.6	2.4
T_c (HJD)..	2454008.73205	0.00028

NOTES.—The parameter values in the second column are the median values of the MCMC distributions, and the uncertainties in the third column are the standard deviations. These are for a *fixed* choice of $M_\star = 0.79\ M_\odot$ and for a *fixed* choice of the limb-darkening function (see the text). The 12% uncertainty in $M_\star$ introduces an *additional* 4% uncertainty in $R_\star$ and R_p (and has no effect on the other parameters).

$\approx$25% of jumps are executed. We created 10 independent chains with 500,000 points each, starting from random initial positions. The first 100,000 points were not used, to minimize the effect of the initial condition. The Gelman & Rubin (1992) R-statistic was close to unity for each parameter, a sign of good mixing and convergence.

5. RESULTS

The model that minimizes χ^2 is plotted as a solid line in Figure 1. The optimized residual extinction correction has been applied to the data that are plotted in Figure 1, and to the data that are given in Table 1. The differences between the observed fluxes and the model fluxes are also shown beneath each light curve.

Tables 3 and 4 give the estimated values and uncertainties for each parameter based on the MCMC analysis. They also include some useful derived quantities: the impact parameter $b = a \cos i/R_\star$; the transit duration (i.e., the elapsed time between first contact $t_{\rm I}$ and last contact $t_{\rm IV}$); and the duration of ingress (i.e., the elapsed time between $t_{\rm I}$ and second contact $t_{\rm II}$). Although the MCMC distributions are not exactly symmetric about the median, Tables 3 and 4 report (with two exceptions) only the median values for the derived parameters and their standard deviations. The exceptions are the impact parameter b and inclination i for WASP-1. Those results are best described as one-sided confidence limits because the data are consistent with a central transit.

There are several sources of systematic error that are not taken into account by the MCMC analysis. The first is the systematic error that results from the covariance between $M_\star$ and both of the parameters R_p and $R_\star$, as discussed in § 4. For WASP-1 we adopted $M_\star = 1.15\ M_\odot$ based on the interpretation by Collier Cameron et al. (2007) of the stellar spectrum. These authors report an uncertainty of about 15% in $M_\star$, which translates into a systematic error of 5% in our estimates of $R_\star$ and R_p. For WASP-2 we adopted $M_\star = 0.79\ M_\odot$, and the uncertainty in $M_\star$ is about 12%, which in turn contributes a 4% error in $R_\star$ and R_p.[7] The other transit parameters (such as b, i, and T_c) do not depend on $M_\star$.

A second potential source of systematic error is the bias due to an incorrect choice of either the limb-darkening function or the values of the limb-darkening coefficients. We investigated the effects of varying the functional form of the limb-darkening law

from quadratic to linear, and of allowing the coefficients to be free parameters rather than holding them fixed, and in all cases we found that the resulting changes to R_p were much smaller than the other sources of error. We conclude that the systematic error in R_p due to the choice of limb-darkening law is small compared to either the statistical uncertainty or the systematic uncertainty due to the covariance with $M_\star$.

6. DISCUSSION

Our estimates for the stellar radii are consistent with, and more precisely determined than, the initial estimates from spectroscopy presented in Collier Cameron et al. (2007). In particular, that paper constrained the stellar radii of WASP-1 and WASP-2 to be $1.04 < R_\star < 1.92$ and $0.72 < R_\star < 0.84$, respectively, whereas we find $R_\star = 1.45 \pm 0.08$ for WASP-1 and $R_\star = 0.81 \pm 0.04$ for WASP-2. These uncertainties include the contribution from the uncertainty in the stellar mass. In the case of WASP-1, the uncertainty in $M_\star$ dominates that from random photometric errors. For WASP-2, these two sources of uncertainty are comparable.

Our revised estimates for R_p for both WASP-1b and WASP-2b are 5 times more precise than those presented in the discovery paper. The three exoplanets WASP-2b, XO-1b (McCullough et al. 2006; Holman et al. 2006), and WASP-1b present an interesting sequence (Fig. 2): their radii differ by as much as 40%, despite their indistinguishable masses. We note that the radius of WASP-2b is in good agreement with published structural models that include both a 20 $M_\oplus$ core of solid material and the effects of stellar insolation (Bodenheimer et al. 2003). The radius of XO-1b is larger, but it can be explained by a coreless model of a similar effective temperature (Fig. 2). In contrast, we find that WASP-1b is significantly larger than such predictions, whether or not a core is included. WASP-1b is not alone in its anomalous size: both HD 209458b (Knutson et al. 2007) and HAT-P-1b (Bakos et al. 2007) also require an additional source of internal energy to account for their large radii. We also note that TrES-2 (O'Donovan et al. 2006) may require such heating as well, depending on the outcome of more precise measurements of the planetary radius.

Only a month ago, HD 209458b was the single known case of a hot Jupiter that is almost certainly too large to be explained by standard models of planetary structure. (The other possible case, OGLE-TR-10, was ambiguous because of the uncertainty in its radius; see Holman et al. 2007). With only one strong anomaly, explanations requiring somewhat improbable events were perfectly viable. However, now that a significant fraction of the transiting hot Jupiters are found to be similarly in need of this additional energy,

----

[7] We note that our formal systematic errors should be asymmetric because Collier Cameron et al. (2007) reported asymmetric error bars on $M_\star$, which we have not taken into account here.
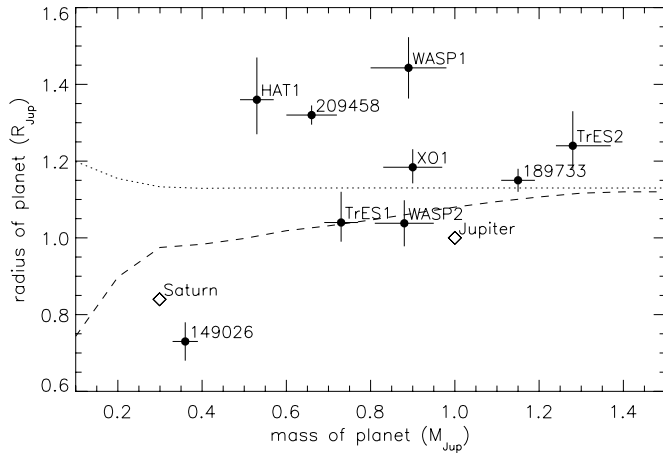
FIG. 2.—Masses and radii for the known transiting extrasolar planets within 300 pc, as well as Jupiter and Saturn for comparison. The dotted line corresponds to the insolated coreless structural models of Bodenheimer et al. (2003) for an age of 4.5 Gyr and a planetary effective temperature of 1500 K. The dashed line shows their models for the same parameters but including the presence of a $20\,M_{\oplus}$ core of solid material. Insolation alone is clearly insufficient to account for the large radii of three of the planets (HAT-P-1b, WASP-1b, and HD 209458b) and likely a fourth (TrES-2), regardless of whether or not a core is present. Interestingly, the parent stars of these four planets are significantly more massive than those of the planets that are in good agreement with the models (TrES-1, WASP-2b, and HD 189733b), all of which orbit lower mass K dwarf stars.

the burden of the theorists may shift to seeking explanations for this effect that are more generally applicable.

Examining Figure 2, we note that the three planets in closest agreement with the published structural models of Bodenheimer et al. (2003) all orbit the lowest mass stars of the sample, namely TrES-1 ($M_{\star} = 0.89 \pm 0.05\ M_{\odot}$; Sozzetti et al. 2004; Alonso et al. 2004; Laughlin et al. 2005b), WASP-2 ($M_{\star} = 0.79^{+0.15}_{-0.04}\ M_{\odot}$), and HD 189733 ($M_{\star} = 0.82 \pm 0.03\ M_{\odot}$; Bouchy et al. 2005; Bakos et al. 2006). In contrast, the host stars of the three largest hot Jupiters all orbit stars more massive than the Sun: WASP-1 ($M_{\star} = 1.15^{+0.24}_{-0.09}\ M_{\odot}$), HAT-P-1 ($M_{\star} = 1.12 \pm 0.09\ M_{\odot}$; Bakos et al. 2007), and HD 209458 ($M_{\star} = 1.10 \pm 0.06\ M_{\odot}$; Knutson et al. 2007). It is likely too soon to search for such patterns in these data: We note that the planet of the most massive star, HD 149026

($M_{\star} = 1.3 \pm 0.1\ M_{\odot}$; Sato et al. 2005), is the smallest of the sample. Nonetheless, we are encouraged that the recent rapid rate of detection of transiting hot Jupiters will soon provide us with a significantly larger sample in which to assess this and other possible correlations.

Another interesting implication of our measurements for WASP-1 and WASP-2 is that they are both particularly favorable targets for efforts to detect reflected light from exoplanets. A positive detection of reflected light would lead to the first empirical determination of an exoplanetary albedo, and perhaps even its phase function. However, the reflected light is typically a minuscule fraction of the direct light from the star, which explains the long list of unsuccessful attempts to measure this signal both in ground-based spectra (Charbonneau et al. 1999; Collier Cameron et al. 2002; Leigh et al. 2003a, 2003b) and space-based photometry (Rowe et al. 2006). Since the points of first and last contact correspond to orbital phase angles that are typically within 10° of opposition, we may estimate the ratio of the planetary flux f_p to that of the star $f_{\star}$ to be $f_p/f_{\star} \simeq p(R_p/a)^2$, where p denotes the wavelength-dependent geometric albedo. For WASP-1 this quantity is $p \times 3.3 \times 10^{-4}$, the most favorable for any known transiting system. The other systems for which favorable planet-to-star contrast ratios are expected are HD 189733 ($p \times 3.1 \times 10^{-4}$), TrES-2 ($p \times 2.8 \times 10^{-4}$), and WASP-2 ($p \times 2.7 \times 10^{-4}$). The contrast ratios for all of these systems are superior to those for the systems that have been studied to date. We note that the long duration of the WASP-1 transit (the consequence of a nearly equatorial transit of a large star) further facilities a search for reflected light, as it increases the total time in which to gather the signal. Binning the data for WASP-1 in Figure 1 would yield, in principle, a photon-noise limited precision of 9.5×10^{-5}, which is sufficient to address large values of p with good statistical significance, should we succeed in obtaining a time series of similar quality spanning a secondary eclipse.

REFERENCES

Alonso, R., et al. 2004, ApJ, 613, L153
Arras, P., & Bildsten, L. 2006, ApJ, 650, 394
Bakos, G. A., et al. 2006, ApJ, 650, 1160
———. 2007, ApJ, 656, 552
Baraffe, I., Chabrier, G., Barman, T. S., Allard, F., & Hauschildt, P. H. 2003, A&A, 402, 701
Bodenheimer, P., Laughlin, G., & Lin, D. N. C. 2003, ApJ, 592, 555
Bodenheimer, P., Lin, D. N. C., & Mardling, R. A. 2001, ApJ, 548, 466
Borucki, W. J., et al. 2003, Proc. SPIE, 4854, 129
Bouchy, F., et al. 2005, A&A, 444, L15
Burrows, A., Sudarsky, D., & Hubbard, W. B. 2003, ApJ, 594, 545
Charbonneau, D., Brown, T. M., Burrows, A., & Laughlin, G. 2007, in Protostars and Planets V, ed. B. Reipurth, D. Jewitt, & K. Keil (Tucson: Univ. Arizona Press), 701
Charbonneau, D., Noyes, R. W., Korzennik, S. G., Nisenson, P., Jha, S., Vogt, S. S., & Kibrick, R. I. 1999, ApJ, 522, L145
Charbonneau, D., et al. 2006, ApJ, 636, 445
Claret, A. 2004, A&A, 428, 1001
Collier Cameron, A., Horne, K., Penny, A., & Leigh, C. 2002, MNRAS, 330, 187
Collier Cameron, A., et al. 2007, MNRAS, 375, 951
Deming, D., Seager, S., Richardson, L. J., & Harrington, J. 2005, Nature, 434, 740

Fortney, J. J., Saumon, D., Marley, M. S., Lodders, K., & Freedman, R. S. 2006, ApJ, 642, 495
Gaudi, B. S. 2005, ApJ, 628, L73
Gelman, A., & Rubin, D. B. 1992, Statistical Science, 7, 457
Gilliland, R. L., et al. 1993, AJ, 106, 2441
Guillot, T., Burrows, A., Hubbard, W. B., Lunine, J. I., & Saumon, D. 1996, ApJ, 459, L35
Holman, M. J., et al. 2006, ApJ, 652, 1715
———. 2007, ApJ, 655, 1103
Knutson, H., Charbonneau, D., Noyes, R. W., Brown, T. M., & Gilliland, R. L. 2007, ApJ, 655, 564
Laughlin, G., Marcy, G. W., Vogt, S. S., Fischer, D. A., & Butler, R. P. 2005a, ApJ, 629, L121
Laughlin, G., Wolf, A., Vanmunster, T., Bodenheimer, P., Fischer, D., Marcy, G., Butler, P., & Vogt, S. 2005b, ApJ, 621, 1072
Leigh, C., Cameron, A. C., Horne, K., Penny, A., & James, D. 2003a, MNRAS, 344, 1271
Leigh, C., Collier Cameron, A., Udry, S., Donati, J.-F., Horne, K., James, D., & Penny, A. 2003b, MNRAS, 346, L16
Lin, D. N. C., Bodenheimer, P., & Richardson, D. C. 1996, Nature, 380, 606
Mandel, K., & Agol, E. 2002, ApJ, 580, L171
McCullough, P. R., et al. 2006, ApJ, 648, 1228
O'Donovan, F. T., et al. 2006, ApJ, 651, L61

Press, W. H., Teukolsky, S. A., Vetterling, W. T., & Flannery, B. P. 1992, Numerical Recipes in C (Cambridge: Cambridge Univ. Press)
Rowe, J. F., et al. 2006, ApJ, 646, 1241
Sato, B., et al. 2005, ApJ, 633, 465
Showman, A. P., & Guillot, T. 2002, A&A, 385, 166
Sozzetti, A., et al. 2004, ApJ, 616, L167
Tegmark, M., et al. 2004, Phys. Rev. D, 69, 103501
Winn, J. N., & Holman, M. J. 2005, ApJ, 628, L159
Winn, J. N., Holman, M. J., & Fuentes, C. I. 2007, AJ, 133, 11
Winn, J. N., et al. 2005, ApJ, 631, 1215